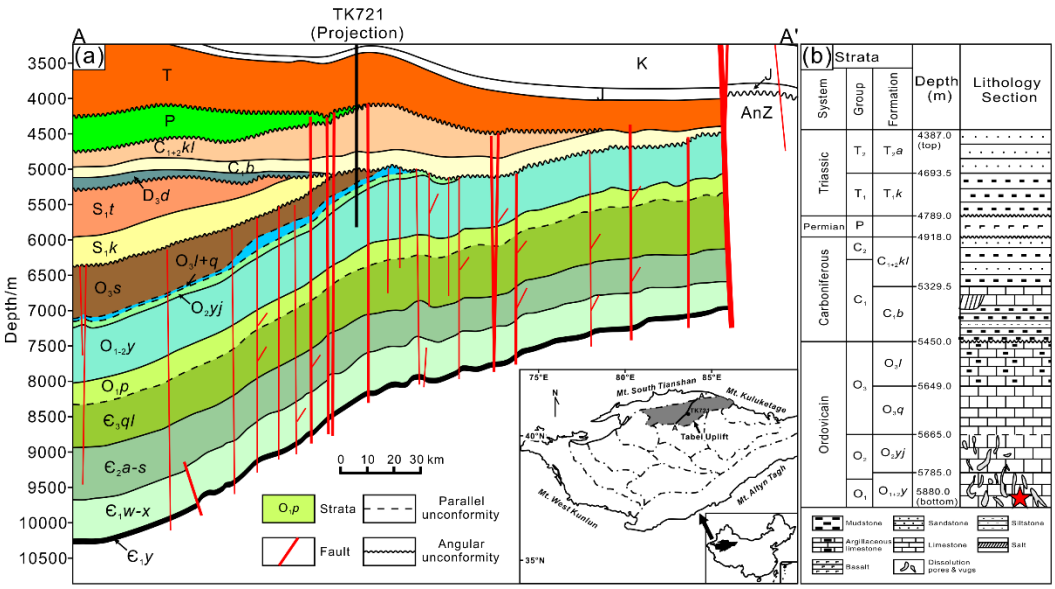


**Figure 1.** (a) Stratigraphic and structural cross section of the Tabei Uplift, Tarim Basin. Inset shows the geographic location of the Tabei Uplift; (b) Generalized stratigraphic column of Well TK721, showing the depths of various stratal boundaries and the position of the sample (red star) studied in this study.

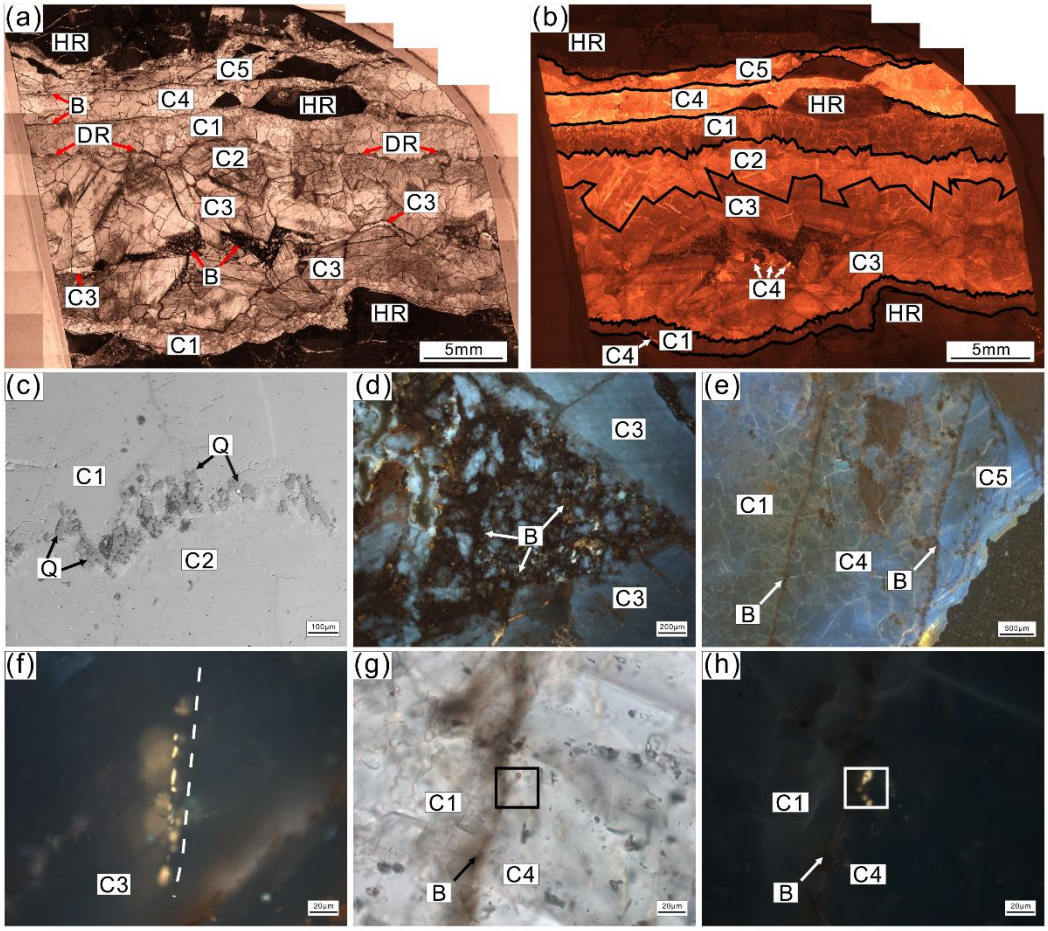


**Figure 2.** Photomicrographs of calcite vein showing the paragenetic relationships of calcite cements, the occurrence of "dust rim", bitumen, and oil inclusions in the Ordovician Yingshan Formation ($O_{1-2}y$). (a) and (b) Photomicrograph mosaics of the calcite vein studied under transmitted light and CL, showing five generations of cement (C1 to C5), HR = host rock, B = bitumen, DR = dust rim; (c) BS-SEM image showing fine-grained detrital quartz (Q) grains filling the "dust rim" between C1 and C2 calcite cements; (d) Photomicrograph showing dissolution of C3 and the presence of bitumen (B); (e) Fluorescence photomicrograph showing bitumen (B) rims between C1 and C4, C4 and C5; (f) Fluorescence photomicrograph showing yellow-orange oil inclusions along an annealed microfracture in C3; (g) and (h) Close-up view of photomicrographs under transmitted light and UV fluorescence showing bitumen (B) and oil inclusions along the C1 and C4 contact.

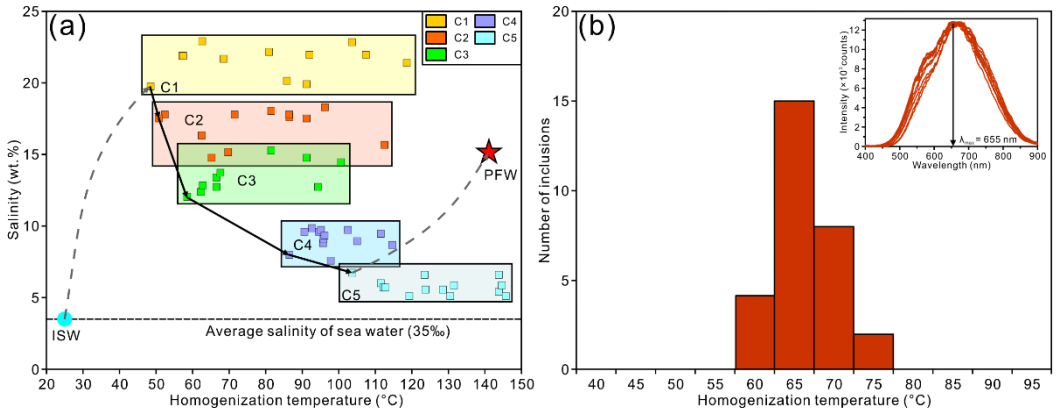


**Figure 3.** Fluid inclusion characteristics within the calcite vein in the Ordovician Yingshan Formation ($O_{1\text{-}2}y$). (a) Cross plot of fluid inclusion salinity vs homogenization temperatures (Th) for the C1-C5 calcite cements, ISW = initial seawater, PFW = present-day formation water. Note that the black solid lines represent the fluid evolution paths of the carbonate reservoir during the Carboniferous, while the gray dotted line represents the inferred fluid evolution path; (b) Histogram of homogenization temperatures (Th) of oil inclusions, showing a confined distribution with a mode of 65–70 ℃. Inset shows fluorescence spectra of individual oil inclusions from the calcite vein, showing a consistent spectral peak around 655 nm.

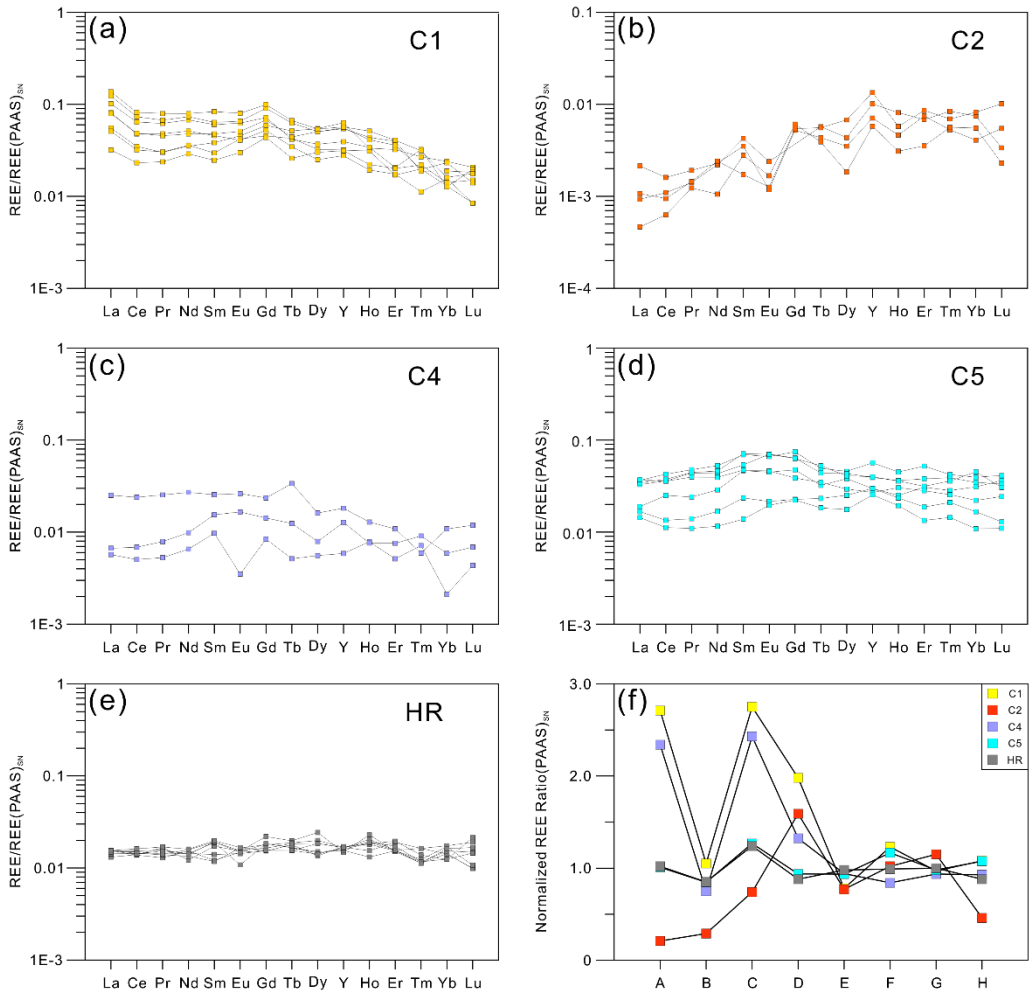


**Figure 4.** REE + Y characteristics for the C1 to C5 calcite cements and host rock in the Ordovician Yingshan Formation ($O_{1\text{-}2}y$). (a)-(e) PAAS-normalized REE + Y patterns for the calcite vein and host rock; (f) Comparison of various REE ratios among various generations of calcite vein and host rock. Note that A-H denote the median of [Pr/Yb], [Pr/Tb], [Tb/Yb], [La/La*], [Ce/Ce*], [Gd/Gd*], [Er/Er*] and [Eu/Eu*] ratios relative to the PAAS-normalization, respectively.

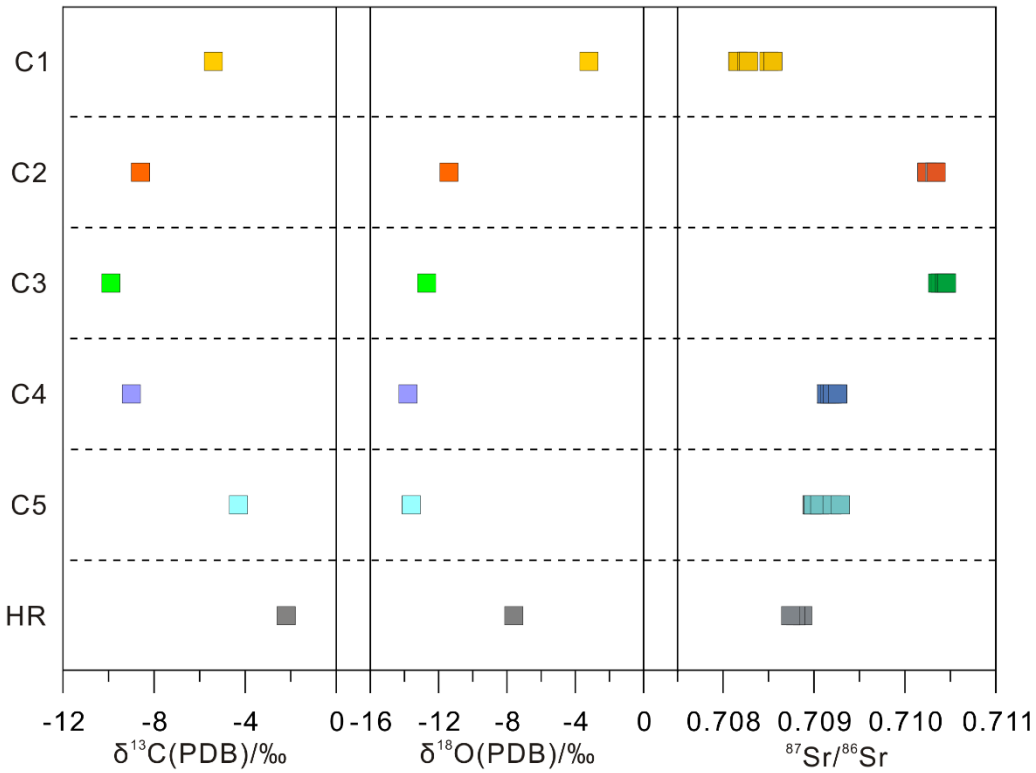


**Figure 5.** Carbon (C), oxygen (O) and strontium (Sr) isotope characteristics for the C1-C5 calcite cements and host rock in the Ordovician Yingshan Formation ($O_{1\text{-}2}y$).

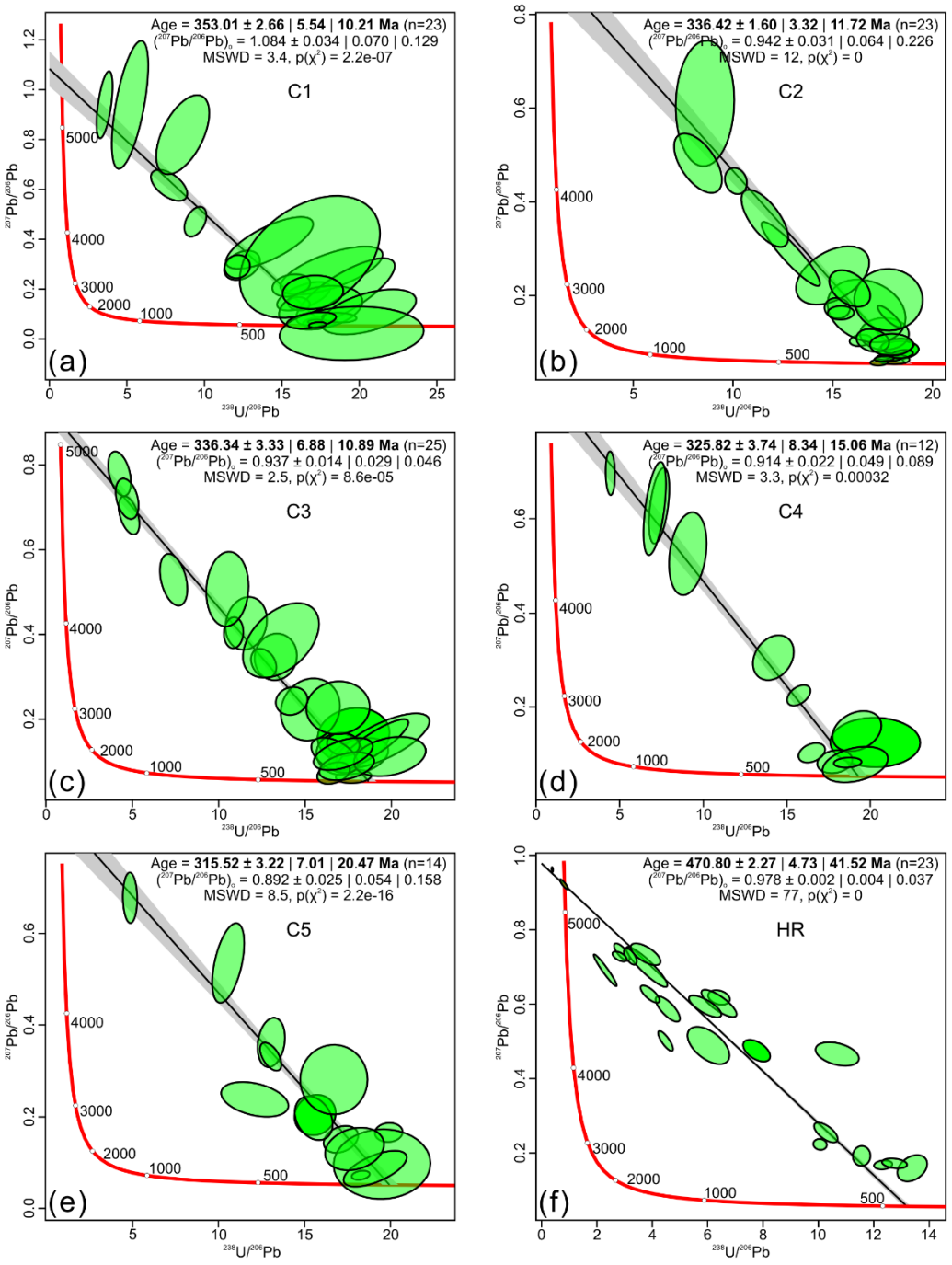


**Figure 6.** (a)-(f) U-Pb Tera-Wasserburg concordia plots for the C1-C5 calcite cements and host rock in the Ordovician Yingshan Formation ($O_{1\text{-}2}y$). The results are reported as t ± x | y | z, where t stands for the age or initial Pb-ratio, x is the standard error, y and z are the (95%) confidence intervals without and with over-dispersion, respectively.

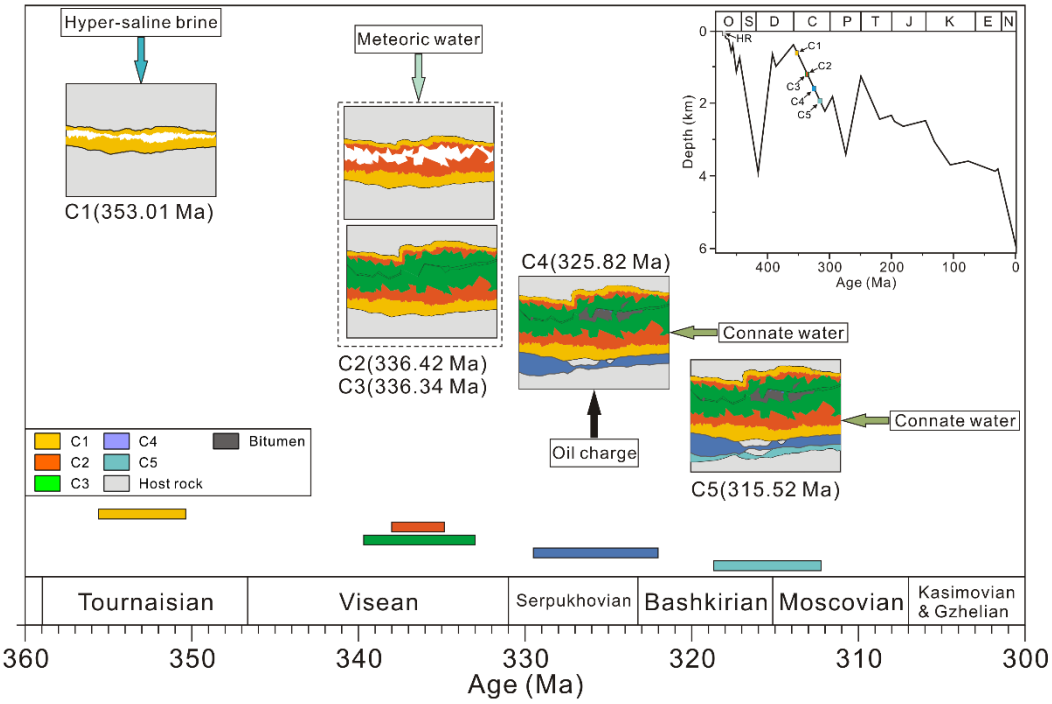


**Figure 7.** Schematic diagram showing the fluid-flow events and formation processes of the C1-C5 calcite cements during the Carboniferous. Insert shows burial history diagram of the studied Ordovician reservoir for comparison (modified from Liu et al., 2017), depicting the relative burial depths of the calcite cement precipitated.

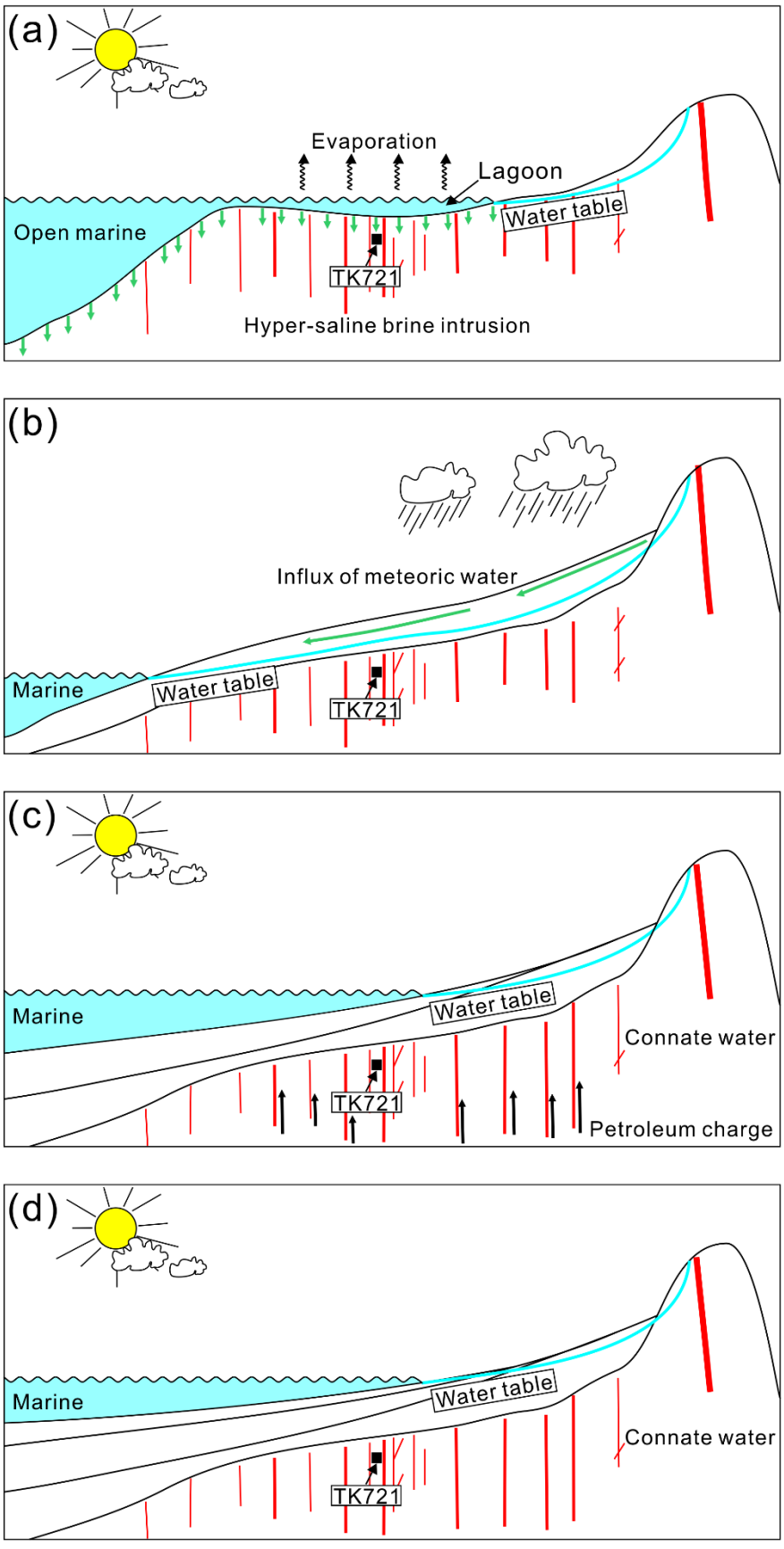


**Figure 8.** Schematic diagrams illustrating fluid evolution history in the studied Ordovician carbonate

reservoir during the Carboniferous. (a) Hyper-saline brine intrusion from the lagoon during the precipitation of C1; (b) Influx of meteoric water into the reservoir during C2 and C3 precipitation; (c) Petroleum charge occurring during the cementation of C4; (d) Reservoir formation water in equilibrium with the Ordovician connate water during the precipitation of C5.